Formation and etching of the insulating Sr-rich V^{5+} phase at the metallic $SrVO_3$ surface revealed by operando XAS spectroscopy characterizations

Vincent Polewczyk,[1,*] Moussa Mezhoud,[2] Martendo Rath,[2] Oualyd El-Khaloufi,[2] Ferdinando Bassato,[1] Arnaud Fouchet,[2] Wilfrid Prellier,[2] Mathieu Frégnaux,[3] Damien Aureau,[3] Luca Braglia,[1] Giovanni Vinai,[1] Piero Torelli,[1] Ulrike Lüders[2]

[1] Istituto Officina dei Materiali (IOM)–CNR, Laboratorio TASC, Area Science Park, S.S.14, km 163.5, I-34149 Trieste, Italy
[2] Normandie Univ, ENSICAEN, UNICAEN, CNRS, CRISMAT, 14000 Caen, France
[3] ILV, CNRS UMR 8180, Université de Versailles Saint-Quentin-en-Yvelines – Université Paris-Saclay, Versailles, France

[*]e-mail: vincent.polewczyk@cea.fr. Current address: Univ. Grenoble Alpes, CNRS, CEASpintec, 38000 Grenoble, France

Abstract

In the search of low cost and more efficient electronic devices, here we investigate the properties of $SrVO_3$ transparent conductor oxide (TCO) thin films, both visible-range optically transparent and highly conductive, and stands as a promising candidate to substitute the standard ITO in a large range of applications. We especially address its surface stability under water (both liquid and vapor) and other gaseous atmospheres. Through an extensive use of spectroscopy characterizations, x-ray photoemission and *operando* x-ray absorption measurements, we observe the formation of a thin Sr-rich V^{5+} layer located at the surface of the $SrVO_3$ layer with aging, and reveal for the first time how it can be removed from the surface by solvating in water atmosphere. The surface recovery is unambiguously associated to an etching process, here spectroscopically characterized in *operando* conditions, allowing to follow the stoichiometric modification under reaction. Once exposed in oxygen atmosphere, the Sr-rich V^{5+} layer forms again, as detected in *operando*. Our findings improve the understanding of aging effects in perovskite oxides, allowing for the development of functionalized thin films in which it is possible to control or to avoid an insulating surface layer. This constitutes an important step towards the large-scale use of V-based TCOs, with possible implementations in future oxide-based electronics.

Keywords: TCO, Thin film, water etching, aging, oxitronic devices.

1. Introduction

Transition metal oxides are widely studied due to their broad range of versatile functionalities arising from the complex interplay between charge, orbital, spin, and lattice degrees of freedom[1–6]. In this family, it was shown that some

composition present two antagonist properties at the same time: high electrical conductivity and visible-range optical transparency. This class of materials is called transparent conductive oxide (TCO). TCOs are already integrated in a wide range of electronic devices, for instance photodetectors, light-emitting diodes, transistors, sensors or photovoltaic devices, as they allow for optically transparent electrical contacts [7,8]. At the moment, the most used TCO is indium-tin-oxide (ITO), [9] although the scarcity of the element leads to highly volatile prices. To overcome this issue, different materials are proposed as alternative such as Al or Ga doped ZnO [10,11] and more recently vanadium perovskite based TCOs $SrVO_3$ (SVO), which possesses similar electrical and optical properties [12–14]. SVO already proved to be a promising candidate in the next functional oxitronic devices for its metal-to-insulator Mott transition [15,16] and for anodes in solid oxide fuel cells [17,18]. This compound has a cubic perovskite structure (a = 0.3842 nm) with a V^{4+} ($3d^1$) electronic configuration. It presents a metallic behavior and an enhanced Pauli paramagnetic character, both for bulk and thin films [19,20]. SVO thin films can be obtained on different substrates [21][22] using various growth methods including hydride molecular beam epitaxy [23], sputtering [21] and more commonly pulsed laser deposition (PLD) [13,15,19,21,24–31]. These studies on SVO were carried out on epitaxial films, while in applications, these are rarely used. The in-depth study of polycrystalline SVO films is not achieved up to now. Both crystalline or polycrystalline SVO have however some limitations that have still to be overcome, specifically the risk of chemical degradation with aging, occurring much faster than in other perovskite oxides such as $SrRuO_3$[32]. The main signs of degradation are surface demixing in Sr-based oxides and V_2O_5[25], Sr-segregation towards the surface[33] and over-oxidization of V in $Sr_2V_2O_7$ or $Sr_3V_2O_8$[25,27,28,30,34,35] occurring at least on the first top layer. All these thermodynamic instabilities near the surface result in a stoichiometric modification of the material, which is detrimental for its use in both Mottronic application and as TCO due to the increase in resistivity[19,30,36].

In this framework, the focus of recent studies was dedicated to the removal of this spurious surface layer to restore the stoichiometric properties. Most of the Sr compounds are soluble in liquid water but with very different rates, much faster for the Sr-rich phases [31,37,38]. Therefore, using water, we expect to remove mostly the Sr-rich phase and probably very few $SrVO_3$. It is rather difficult to find a solubility rate in literature but typical measurements done by Bourlier *et al.*[39] allow to evaluate roughly a solubility rate of 0.05 $nm.s^{-1}$ when the Sr-rich phase is immerged in liquid deionized water. This procedure may thus represent a low cost and ecologically sustainable treatment ideal for future applications [31,37]. At present, a spectroscopic investigation of the chemical modifications taking place at the surface of $SrVO_3$ in both oxidizing and water environments is missing. Here we firstly report an *operando* characterization of

the $SrVO_3$ surface under ambient pressures, allowing to get insights into the dynamics of the surface modification under realistic conditions.

In this work, we have deposited by Pulsed Laser Deposition (PLD) 55 nm thick polycrystalline SVO films on a Silicon (001) substrate, ideal for further industrial transfer. Then, we artificially aged the sample via *ex situ* annealing treatment in air at 200°C in order to reach a stable surface. In a first step, we have performed spectroscopic measurements with x-ray photoemission (XPS) and x-ray absorption (XAS) techniques in ultra-high vacuum (UHV) conditions to have insights on the chemistry of the aged SVO film surfaces. After having identified the presence of a thin deteriorated surface phase, we cleaned the surface of the sample at ambient pressure with water, both in its vapor and liquid forms, and we further studied for the very first time its dynamics by means of *operando* XAS measurements under ambient pressure. The use of water vapor, to our knowledge up to now unreported in literature, helps to slow down the chemical cleaning and makes an *operando* characterizations possible with our setup. Starting from a freshly etched stoichiometric SVO, we then studied the effects of annealing treatment in different atmospheres, until recovering the initial aged state. Our findings constitute an important step in the understanding of the thermodynamic surface instabilities of $SrVO_3$ and how surface solvation restores stoichiometric properties after aging in ambient atmosphere, a critical step necessary for further technological implementation in oxitronic devices.

2. Experimental details

Si (001) substrates were cleaned with acetone and ethanol in an ultrasonic bath before being introduced in the deposition apparatus. A TiO_2 thin film of about 8 nm has been first deposited by PLD as a seed layer for the crystallization of the 55 nm thick polycrystalline SVO film on top of it. The deposition parameters of both TiO_2 and SVO layers were the same; a KrF excimer laser of 248 nm wavelength, a laser repetition rate of 5 Hz, a substrate to target distance of 40 mm, a deposition pressure of about 1×10^{-6} mbar and a substrate temperature of 600 °C. *Ex situ* artificial aging has then been performed, heating up the structure to 200°C in air for 10 minutes[36]. The intention of this initial aging treatment is to form a reproducible insulating V^{5+} surface layer, with a controlled and accelerated aging process (see **Figure S1**), which also stabilizes the underlying SVO film. On the sample, grazing incident x-ray diffraction (GIXRD, see **Figure S2**) and reflectivity measurements were conducted to investigate the crystallinity and the thickness of the SVO film, respectively. The relatively low annealing temperature used to speed up the aging barely affects the film SVO crystallinity [36].

At the NFFA APE-HE beamline of the Elettra synchrotron radiation facility[40], XPS measurements were then performed in UHV with linearly polarized radiation of 900 eV photon energy, corresponding to a probing depth of around 1 nm. The photoemission spectra were measured at room temperature (RT), with the sample surface oriented at 45° with respect to the incident photon beam and normal to the analyzer axis. The binding energies of the photoemission peaks were calibrated with respect to the Fermi level of an Au reference sample. Core levels were background subtracted by the Shirley function and then fitted using a standard Voigt function with L/G = 20. The atomic concentration was computed using the Thermofisher Scientific Avantage© software and the sensitivity factors tabulated in [41]. XAS measurements at V-$L_{2,3}$ and O-*K* edges were recorded at RT under UHV in total electron yield (TEY) mode, with the same incident angle of 45°, corresponding to a probing depth of around 5 nm, and normalized to the incident photon flux. The spectra were further corrected using the Au reference sample to remove instrumental artifacts across the O-*K* edge. To obtain information on the surface cleaning dynamics and on the surface instabilities, we performed *operando* XAS measurements at ambient atmosphere using the setup described in[42], with the sample placed normal to the incident beam. Due to the increased noise at ambient pressure, we imposed the pre-V-L_3 edge and the high-energy tail of the V-L_2 edge to the same intensity for all the presented spectra. For this, we removed a combined spline plus two-step-like background for edge-jump. A negative bias of 100 V is applied to the sample to accelerate the ejected electrons towards a membrane that collects the absorption signal, being separated from the sample by a few hundreds of μm upon flux of gas. In this setup, a Joule resistance allows to heat the sample up to the desired temperature of 200°C. Gas lines allow to introduce different atmospheres such as H_2O, He, CO and O_2 at ambient pressure and at different concentrations and fluxes.

3. Results & discussions

To obtain information on the chemical state of the aged SVO layer, XPS survey (**Figure 1** (a)), O1s and V2p (**Figure 1** (b)) as well as Sr3d (**Figure 1** (c)) core levels measurements have been used.

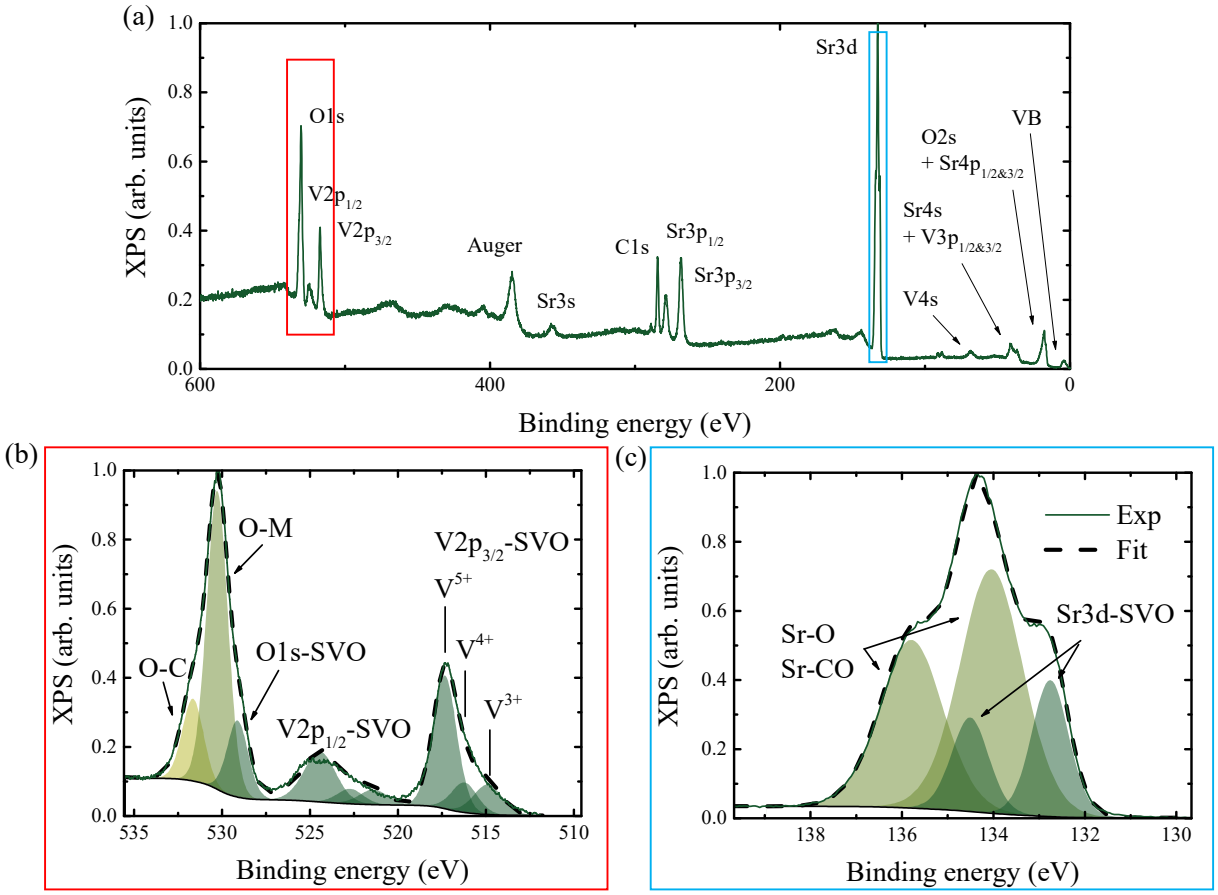

Figure 1. RT XPS survey (a), O1s and V2p (b) and Sr3d (c) measurements collected in UHV on the aged SVO sample and using an incident energy of 900 eV. Fitting of the core levels are also presented with different colors and the overall results are presented in black dotted lines.

All the peaks of the involved elements of SVO are present over the survey scan (Figure 1 (a)). Due to the artificial aging procedure done in air, a non-negligible C 1s surface contamination is detected. The O 1s core level presents multiple contributions (Figure 1 (b)), one on each energy side of the main peak. The lowest energy peak could be attributed to the SrVOx perovskite compound (dark green). The main peak (green) is related to the oxygen coming from the metal-hydroxide (O-M) present at the topmost surface, which is associated here to Sr-O and/or Sr-OH phases, resulting from a Sr-rich surface of the as-grown SVO thin film [25]. The last contribution named O-C (light green) is related to oxygen coming of organic surface contamination and physisorbed species. On the other hand, the V 2p analysis is more delicate due to final state effects, *i.e.* the electron screening that modifies the potential of valence

electrons due to the created core hole occurring in metallic SVO, which results in different observed oxidization states. Their presence does not necessarily imply the existence of spatially localized ions of different oxidation states nor of separate phases because they can be observed even in phase-pure samples. A fine analysis of the intensity, energy position and full width at half maximum ratio should be taken into account as done in reference [35]. Here, the spin orbit splitting between the main peaks ($2p_{1/2}$ and $2p_{3/2}$) and their binding energy positions reveal however a majority V^{5+} state (dark green), which is related either to an over-oxidized V phase such as $Sr_2V_2O_7$ or $Sr_3V_2O_8$, or to demixed V_2O_5, all electrically insulating at RT. The Sr 3d core level presents a broad spectral shape with one central peak plus two extra ones on each energy side. A single doublet should be expected from a pure 3d state, which can be further decomposed with a Sr^{2+} contribution due to the non-stoichiometric SrVOx phases (dark green) and a broader one at higher binding energies (1-1.2eV) (green) coming from Sr-segregated phases such as SrO or $SrCO_3$[25,31], which has a strong affinity with CO_2 present in air. The broadening of the SrO-$SrCO_3$ phase rather than $SrVO_x$ underlayer is most probably due to a difference of charging effect or a lower crystallization of the top deteriorated surface. From the full analysis of the core levels, we found a Sr-rich surface with a global Sr/V ratio of around 3 ± 0.3. This large error bar comes from the choice of Shirley background for a wide spectral region that appears well-adapted here to better adjust the experimental line, but tends to underestimate the XPS vanadium content, as explained in[25]. All these detailed analyses allow to assign unambiguously the presence of a V^{5+} state at the surface in addition to a Sr-rich phase, stemming from the aging process in air exposure [28,30,35].

To avoid misleading in the analysis of the V oxidization state but also to probe deeper the chemical state of the aged SVO sample, XAS measurement at V-$L_{2,3}$ and O-K edges of the aged SVO film have been carried out in UHV conditions. The normalized recorded spectrum is shown in **Figure 2**.

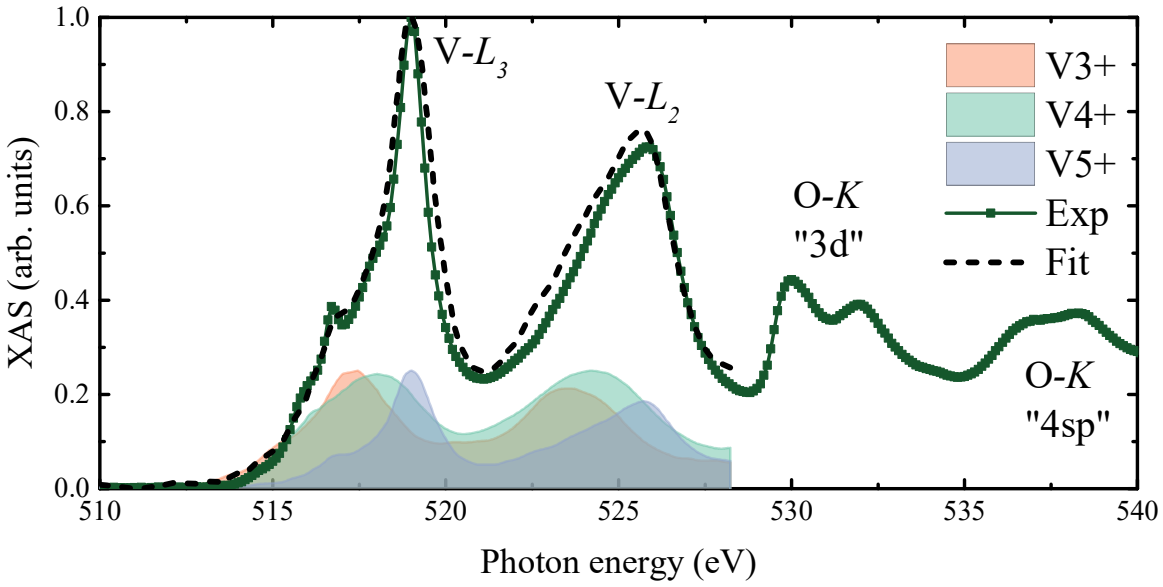

Figure 2. RT XAS spectra collected in UHV on the aged SVO sample. The spectrum is normalized to the V-L_3 edge. Reference spectra of the different oxidization states were digitalized from[43] *and are added in the graph to help at the comparison. A linear combination fit done using these references is also presented in black dotted line.*

The measured spectra in Figure 2 reveal a sharp V-L_3 edge, anticipated by multiple shoulder peaks, then followed by a broader V-L_2 edge. A O-K absorption signal is observed in the high-energy region, indicating the existence of a large number of unoccupied O-*2p* states due to pronounced hybridization-induced transfer of O-*2p* electrons into V-*3d* and V-*4sp* orbitals[44–48]. By calculating the linear combination of the spectral features of similar reference VO_x spectra[43,46,49], without any background subtraction, we succeed to reproduce our experimental spectrum in its main features. The V^{5+} oxidation state is the main contribution of the recorded XA spectra, with a pre-edge observed around 516 eV. The presence of V^{3+} is unambiguously ruled out, as expected from chemical considerations of over-oxidized phases of $SrVO_3$. The low, but finite intensity in the XPS analysis (see Figure 1 (b)) is indeed related to final state effects. The fits using the references indicate a minimum contribution of V^{5+} of 80%, while only 20% of the spectra can be attributed to V^{4+}, the oxidation state expected in stoichiometric $SrVO_3$. This low contribution of V^{4+} confirms the findings of the XPS analysis, with Sr-rich V^{5+} phases at the topmost part of the layer, but due to the slightly deeper probing depth of XAS, a stoichiometric $SrVO_3$ phase may still be present below the chemically modified top surface.

After having identified the chemical state of the deteriorated surface layer of aged SVO, we probed the effect of liquid water cleaning, with the aim of recovering the V^{4+} state at the surface, by repeating XPS (see **Figure 3**) and XAS (see **Figure S3** focused on the V-$L_{2,3}$ edges) characterizations after immerging and agitating the sample by hand in deionized water for 1 minute and reintroducing it in the measurement apparatus.

No additional elements are observed on the XPS survey scans before and after the liquid water treatment in Figure 3 (a). The shape and the energy positions of the core levels reveal however important differences, as it can be observed in Figure 3 (b) and (c). Using a careful fit analysis, the main contribution to the O 1s peak is attributed to $SrVO_3$, with a small shoulder at higher binding energies due to from O-M / O-C states (see Figure 3 (d)). The main contribution to the V 2p levels (Figure 3 (d)) is related now to the V^{4+} state, while the V^{5+} and the V^{3+} contributions are smaller. In Figure 3 (e), the Sr 3d core level has also drastically evolved, showing a prominent Sr^{2+} character with two sharp peaks, in contrast with the broader peak present before water treatment. A small contribution from surface contaminations, either due to a non-complete surface recovery or to adventitious adsorbates attached to the surface during the short transfer of the washed sample to the UHV chamber, is still detected in all core levels. From the full analysis of the core levels, we found a global Sr/V ratio of around 1.2 ± 0.3, which corresponds to stoichiometric $SrVO_3$. The XAS spectra in **Figure S3** reveal similar behavior with a clear evolution from a V^{5+} to a V^{4+} state, with an increase of the V-L_3 pre-edge but also with an enhancement of V-L_2 edge intensity, *i.e.* towards the state expected for stoichiometry $SrVO_3$. While the V-L_3 edge shifts towards a lower photon energy by approximatively 0.2 eV, the V-L_2 edge shows a larger shifts, reflecting a smaller spin-orbit splitting for this V^{4+} state as already observed in other studies on VO_x materials [50,51]. Therefore, both XPS and XAS results point to the presence of a mostly stoichiometric $SrVO_3$ surface after the water bath of 1 minute, being sufficient to remove the chemically modified aged surface. As shown in a previous study [36], we can consider the thickness of the modified top layer to be 3 nm thick, resulting in an etching rate of 0.05 $nm.s^{-1}$, consistent with literature[39].

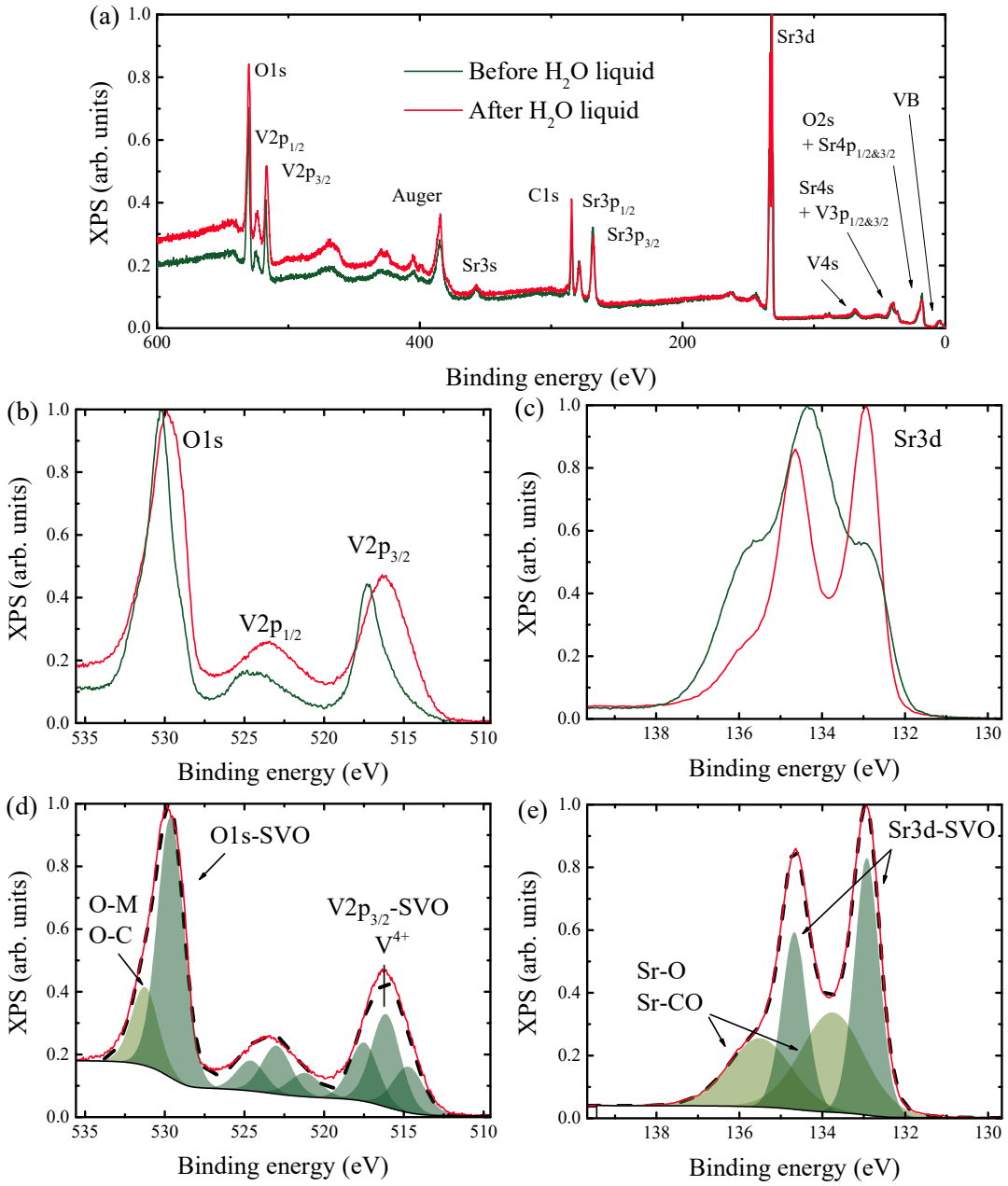

Figure 3. RT XPS (survey (a), O1s and V2p (b and d) and Sr3d (c and e)) spectra recorded before (dark green) and after liquid water cleaning procedure of 1 minute (red). Fitting of the core levels are also presented with the same color code than Figure 1 for the spectra recorded after liquid water treatment.

However, this value is only a lower estimation, as the necessary minimal duration of the water bath to dissolve the top layer has not been determined. Such experiments are laborious due to the necessary transfers from the water bath to

the UHV measurement chamber, which is the reason for investigating the dissolution of the modified top layer with water vapor, *i.e.* slowing down the reaction by reducing the amount and interactions of water on the surface of the sample. This was done by fluxing 3% of water vapor in 50 sccm of He atmosphere onto the sample surface during 130 minutes, reaching ambient pressure in the *operando* XAS setup and therefore conditions as near as possible to ambient exposition.

We first confirm the etching of the aged SVO surface with water vapor by performing reflectivity measurements (see **Figure 4**).

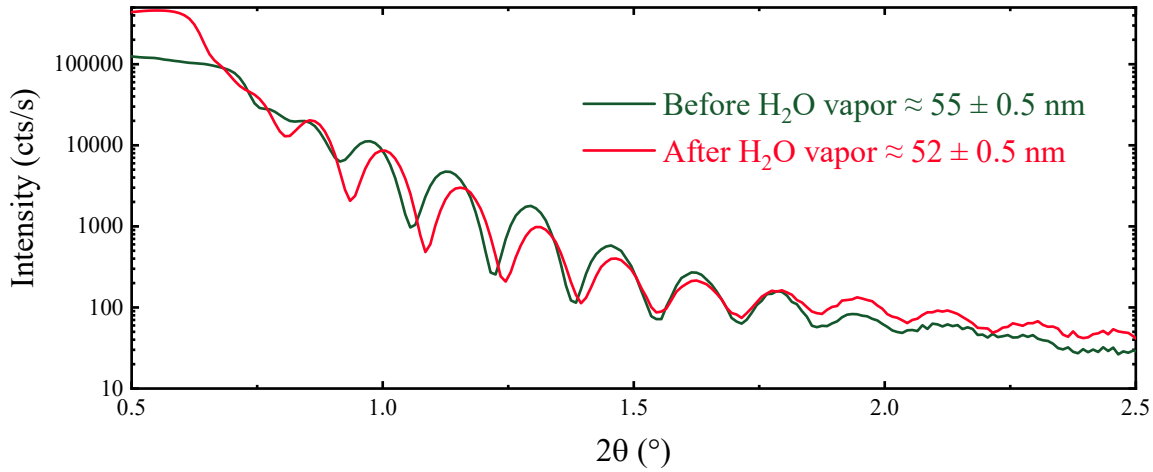

Figure 4. X-ray reflectivity measurements performed on the aged SVO sample before (dark green) and after (red) the water vapor cleaning treatment.

The experimental curves collected before and after water vapor treatment show well defined oscillations on a long 2θ range. After water vapor exposure, the longer intensity oscillation period indicates a thickness reduction of around 3 nm with no detected effects on surface roughness. The similar slope of the curves shows a similar surface roughness compared to the aged sample. However, the critical angle is reduced after the water vapor exposition, translating a change in electron density of the film, probably related to the absence of the chemically modified top layer.

We also performed *operando* XAS characterizations using the same vapor water parameters, measuring simultaneously the evolution of V-$L_{2,3}$ edges during the exposure (see **Figure 5** (a)). The evolution of V^{4+}/V^{5+} obtained after performing linear combination fits is exposed in **Figure 5** (b).

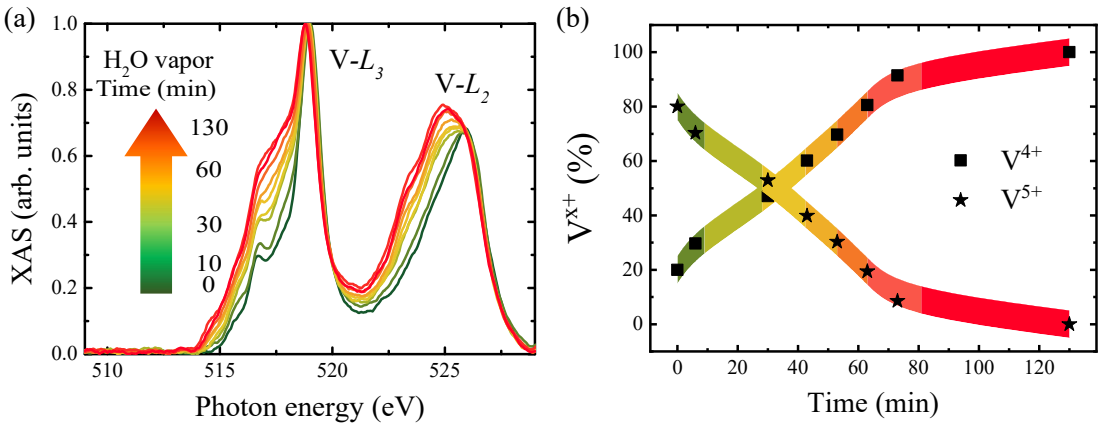

Figure 5. (a) Operando XAS spectra of the V-$L_{2,3}$ edges collected at RT, during the exposure of the sample surface to 3% of water vapor in 50 sccm of He fluxed at ambient pressure. The initial state (green curve) corresponds to the aged SVO sample presented in Figure 3. (b) Elemental concentration of V^{4+}/V^{5+} (squares/stars) as a function of time, including error bars.

Similarly to the case of a liquid water cleaning, we observe an evolution from V^{5+} to a V^{4+} state, with a consistent increase of the V-L_3 pre-edge and V-L_2 edge intensities combined with a large shift of the V-L_2. No drastic multiplet differences can be observed in the intermediate states, proving a smooth second-order transition. As it can be seen in Figure 5 (a and b), 3% water vapor is enough to induce a full surface layer removal, with few changes during the first minutes of exposure and a full removal after around 60 minutes. In these cleaning conditions, the etching rate has been evaluated as approximatively 0.001 $nm.s^{-1}$, and makes the water vapor cleaning at least 50 times slower than the liquid water one. The water vapor needs time to condensate on the surface, forming most probably a very thin layer of water as seen in reference[52], before solvating and surrounding the V sites. We believe that the He flux helps in mechanically removing the formed solvated drops at the surface, similarly to the cleaning/etching process which takes place in the case of liquid water. To the best of our knowledge, this is the first time that a chemical etching is probed by *operando* XAS characterizations.

Finally, the thermodynamic stability of the freshly cleaned SVO surface has been investigated by using a similar procedure to the aging treatment, *i.e.* an annealing at 200°C at ambient pressure, in different atmospheres. First, as

shown in **Figure 6**, we heated up the sample at 200°C in a neutral He (50sccm) atmosphere and tracked the spectra evolution in time. At the same temperature, a reducing CO atmosphere (2 up to 10 sccm) was then fluxed, followed by an oxidizing O_2 atmosphere (2 sccm).

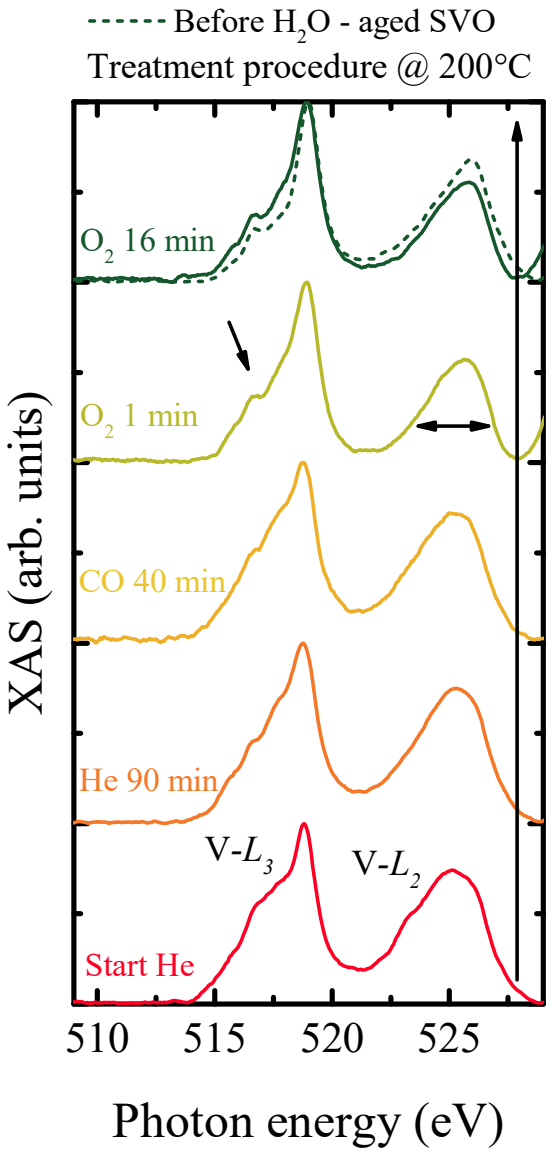

Figure 6. Subsequent Operando XAS spectra recorded at 200°C in different atmospheres: He (50sccm) during 90 minutes, then a mix of He(50sccm)+CO(2sccm) during 40 minutes and lastly a mix of He(50sccm)+O_2(2sccm) during 16 minutes. The initial spectrum of the aged sample shown in Figure 5 is also added here for comparison as a dashed green line.

During the first step, remaining in neutral He atmosphere for tens of minutes at elevated temperature affects only very slightly the stable stoichiometric SVO state (see red and orange curves in Figure 6). Small changes on the pre-L_3 edge are observed and are attributed to small readjustments of the local symmetry and of the electron density due to crystal field effects[53]. In the following reducing condition, fluxing 2 up to 10 sccm (not shown here) CO gas for 40 min gives no chemical variation (see yellow curve Figure 6). This is expected since V^{3+} state is unlikely to form in SVO compounds, except in case of Sr dissociation with V_2O_3[54]. Finally, the presence of an oxidizing atmosphere (see green curves in Figure 6) changes very quickly the surface chemical state as highlighted by arrows, reaching the aged SVO V^{5+} state after only 1 minute of exposition in 2 sccm of O_2, and with no further major changes in the following minutes. Here, the green dashed spectrum, corresponding to the *ex-situ* aged sample of Figure 5 before water treatment, is added for comparison, confirming the almost complete transition to an Sr-rich V^{5+} phase after only 16 minutes of exposure in He(50sccm)+O_2(2sccm) atmosphere. This last measurement indicates the quick dynamics of the oxidation effect and proves the full reversibility of the formation of a thin deteriorated phase at the metallic $SrVO_3$ surface.

4. Conclusion

By an extensive use of multi-spectroscopic characterizations both in UHV and in ambient pressure, we first highlight the thermodynamic instability of the transparent conductive SVO thin film surface, with the appearance of a few nm thick insulating Sr-rich V^{5+} with aging. This spurious phase can however be removed via a water cleaning, effective both in liquid and vapor form. In the latter case, the slower dynamic allows to probe *operando* the evolution of the V-edges in time induced by both surface solvation and oxygen exposure, up to now unreported in literature. The cleaning has been unambiguously associated to the etching of the thin Sr-rich V^{5+} phase, limited to the very first nm of the sample surface and therefore not particularly detrimental for possible implementation in devices. When annealed under different atmospheres, we reveal a quick formation of the Sr-rich phase under oxidizing atmosphere at a moderate temperature of 200°C. These *operando* XAS characterizations allow following the stoichiometric evolution under operative conditions, and pave the way for further investigations with SVO integrated on possible devices. In addition, our results constitute an important step in the understanding of the thermodynamic instability of V-based TCO. The reproducible use of a low cost and ecologically sustainable treatment with water makes this TCO ideal for future applications.

Acknowledgements

This work has been partially performed in the framework of the Nanoscience Foundry and Fine Analysis (NFFA-MUR Italy Progetti Internazionali) facility (https://www.trieste.nffa.eu/). Financial support by the Normandy region is acknowledged, through the projects Cibox and PLDsurf, as well as the PhD project pTCO.

References

[1] M. Coll, J. Fontcuberta, M. Althammer, M. Bibes, H. Boschker, A. Calleja, G. Cheng, M. Cuoco, R. Dittmann, B. Dkhil, I. El Baggari, M. Fanciulli, I. Fina, E. Fortunato, C. Frontera, S. Fujita, V. Garcia, S. T. B. Goennenwein, C.-G. Granqvist, J. Grollier, R. Gross, A. Hagfeldt, G. Herranz, K. Hono, E. Houwman, M. Huijben, A. Kalaboukhov, D. J. Keeble, G. Koster, L. F. Kourkoutis, J. Levy, M. Lira-Cantu, J. L. MacManus-Driscoll, J. Mannhart, R. Martins, S. Menzel, T. Mikolajick, M. Napari, M. D. Nguyen, G. Niklasson, C. Paillard, S. Panigrahi, G. Rijnders, F. Sánchez, P. Sanchis, S. Sanna, D. G. Schlom, U. Schroeder, K. M. Shen, A. Siemon, M. Spreitzer, H. Sukegawa, R. Tamayo, J. van den Brink, N. Pryds, F. M. Granozio, *Appl. Surf. Sci.* **2019**, *482*, 1.

[2] M. Lorenz, M. S. Ramachandra Rao, T. Venkatesan, E. Fortunato, P. Barquinha, R. Branquinho, D. Salgueiro, R. Martins, E. Carlos, A. Liu, F. K. Shan, M. Grundmann, H. Boschker, J. Mukherjee, M. Priyadarshini, N. DasGupta, D. J. Rogers, F. H. Teherani, E. V Sandana, P. Bove, K. Rietwyk, A. Zaban, A. Veziridis, A. Weidenkaff, M. Muralidhar, M. Murakami, S. Abel, J. Fompeyrine, J. Zuniga-Perez, R. Ramesh, N. A. Spaldin, S. Ostanin, V. Borisov, I. Mertig, V. Lazenka, G. Srinivasan, W. Prellier, M. Uchida, M. Kawasaki, R. Pentcheva, P. Gegenwart, F. Miletto Granozio, J. Fontcuberta, N. Pryds, *J. Phys. D. Appl. Phys.* **2016**, *49*, 433001.

[3] G. M. Pierantozzi, G. Vinai, A. Y. Petrov, A. De Vita, F. Motti, V. Polewczyk, D. Mondal, T. Pincelli, R. Cucini, C. Bigi, I. Vobornik, J. Fujii, P. Torelli, F. Offi, G. Rossi, G. Panaccione, F. Borgatti, *J. Phys. Chem. C* **2021**, acs. jpcc.1c02323.

[4] A. Dmitriyeva, V. Mikheev, S. Zarubin, A. Chouprik, G. Vinai, V. Polewczyk, P. Torelli, Y. Matveyev, C. Schlueter, I. Karateev, Q. Yang, Z. Chen, L. Tao, E. Y. Tsymbal, A. Zenkevich, *ACS Nano* **2021**, *15*, 14891.

[5] J. Dho, Y. N. Kim, Y. S. Hwang, J. C. Kim, N. H. Hur, *Appl. Phys. Lett.* **2003**, *82*, 1434.

[6] P. Zubko, S. Gariglio, M. Gabay, P. Ghosez, J.-M. Triscone, *Annu. Rev. Condens. Matter Phys.* **2011**, *2*, 141.

[7] K. Nomura, H. Ohta, A. Takagi, T. Kamiya, M. Hirano, H. Hosono, *Nature* **2004**, *432*, 488.

[8] M. Segev-Bar, H. Haick, *ACS Nano* **2013**, *7*, 8366.

[9] K. Ellmer, *Nat. Photonics* **2012**, *6*, 809.

[10] I. Valenti, S. Benedetti, A. di Bona, V. Lollobrigida, A. Perucchi, P. Di Pietro, S. Lupi, S. Valeri, P. Torelli, *J. Appl. Phys.* **2015**, *118*, 165304.

[11] M. Gabás, P. Torelli, N. T. Barrett, M. Sacchi, J. R. Ramos Barrado, *APL Mater.* **2014**, *2*, 012112.

[12] J. Laverock, M. Gu, V. Jovic, J. W. Lu, S. A. Wolf, R. M. Qiao, W. Yang, K. E. Smith, *Nano Futur.* **2017**, *1*, 031001.

[13] A. Fouchet, J. E. Rault, M. Allain, B. Bérini, J.-P. Rueff, Y. Dumont, N. Keller, *J. Appl. Phys.* **2018**, *123*, 055302.

[14] L. Zhang, Y. Zhou, L. Guo, W. Zhao, A. Barnes, H. T. Zhang, C. Eaton, Y. Zheng, M. Brahlek, H. F. Haneef, N. J. Podraza, M. H. W. Chan, V. Gopalan, K. M. Rabe, R. Engel-Herbert, *Nat. Mater.* **2016**, *15*, 204.

[15] A. Fouchet, M. Allain, B. Bérini, E. Popova, P.-E. Janolin, N. Guiblin, E. Chikoidze, J. Scola, D. Hrabovsky, Y. Dumont, N. Keller, *Mater. Sci. Eng. B* **2016**, *212*, 7.

[16] M. Gu, S. A. Wolf, J. Lu, *Adv. Mater. Interfaces* **2014**, *1*, 1300126.

[17] J. Macías, A. A. Yaremchenko, D. P. Fagg, J. R. Frade, *Phys. Chem. Chem. Phys.* **2015**, *17*, 10749.

[18] A. A. Yaremchenko, B. Brinkmann, R. Janssen, J. R. Frade, *Solid State Ionics* **2013**, *247–248*, 86.

[19] J. A. Moyer, C. Eaton, R. Engel-Herbert, *Adv. Mater.* **2013**, *25*, 3578.

[20] M. Onoda, H. Ohta, H. Nagasawa, *Solid State Commun.* **1991**, *79*, 281.

[21] D. H. Jung, H. S. So, H. Lee, *J. Vac. Sci. Technol. A* **2019**, *37*, 021507.

[22] M. Mirjolet, H. B. Vasili, A. Valadkhani, J. Santiso, V. Borisov, P. Gargiani, M. Valvidares, R. Valentí, J. Fontcuberta, *Phys. Rev. Mater.* **2021**, *5*, 095002.

[23] M. Brahlek, L. Zhang, C. Eaton, H.-T. Zhang, R. Engel-Herbert, *Appl. Phys. Lett.* **2015**, *107*, 143108.

[24] F. Macià, M. Mirjolet, J. Fontcuberta, *J. Magn. Magn. Mater.* **2022**, *546*, 168871.

[25] Y. Bourlier, M. Frégnaux, B. Bérini, A. Fouchet, Y. Dumont, D. Aureau, *Appl. Surf. Sci.* **2021**, *553*, 149536.

[26] A. Boileau, A. Cheikh, A. Fouchet, A. David, R. Escobar-Galindo, C. Labbé, P. Marie, F. Gourbilleau, U. Lüders, *Appl. Phys. Lett*. **2018**, *112*, 021905.

[27] M. Mirjolet, H. B. Vasili, Ll. López-Conesa, S. Estradé, F. Peiró, J. Santiso, F. Sánchez, P. Machado, P. Gargiani, M. Valvidares, J. Fontcuberta, *Adv. Funct. Mater.* **2019**, *29*, 1904238.

[28] B. Bérini, V. Demange, M. Bouttemy, E. Popova, N. Keller, Y. Dumont, A. Fouchet, *Adv. Mater. Interfaces* **2016**, *3*, 1600274.

[29] S. Backes, T. C. Rödel, F. Fortuna, E. Frantzeskakis, P. Le Fèvre, F. Bertran, M. Kobayashi, R. Yukawa, T. Mitsuhashi, M. Kitamura, K. Horiba, H. Kumigashira, R. Saint-Martin, A. Fouchet, B. Berini, Y. Dumont, A. J. Kim, F. Lechermann, H. O. Jeschke, M. J. Rozenberg, R. Valentí, A. F. Santander-Syro, *Phys. Rev. B* **2016**, *94*, 1.

[30] R. C. Germanicus, Y. Bourlier, V. Notot, B. Bérini, V. Demange, M. Berthe, A. Boileau, M. Euchin, Y. Dumont, D. Aureau, M. Fregnaux, B. Grandidier, U. Lüders, A. David, W. Prellier, L. Biadala, A. Fouchet, *Appl. Surf. Sci.* **2020**, *510*, 145522.

[31] Y. Bourlier, M. Frégnaux, B. Bérini, A. Fouchet, Y. Dumont, D. Aureau, *ChemNanoMat* **2019**, *5*, 674.

[32] H. N. Lee, H. M. Christen, M. F. Chisholm, C. M. Rouleau, D. H. Lowndes, *Appl. Phys. Lett.* **2004**, *84*, 4107.

[33] B. Koo, K. Kim, J. K. Kim, H. Kwon, J. W. Han, W. C. Jung, *Joule* **2018**, *2*, 1476.

[34] Z. Cheng, S. Zha, L. Aguilar, M. Liu, *Solid State Ionics* **2005**, *176*, 1921.

[35] C. Lin, A. Posadas, T. Hadamek, A. A. Demkov, *Phys. Rev. B* **2015**, *92*, 035110.

[36] M. Rath, M. Mezhoud, O. El Khaloufi, O. Lebedev, J. Cardin, C. Labbé, F. Gourbilleau, V. Polewczyk, G. Vinai, P. Torelli, A. Fouchet, A. David, W. Prellier, U. Luders, *submitted*.

[37] Y. Bourlier, B. Bérini, M. Frégnaux, A. Fouchet, D. Aureau, Y. Dumont, *ACS Appl. Mater. Interfaces* **2020**, *12*, 8466.

[38] T. Ohnishi, K. Shibuya, M. Lippmaa, D. Kobayashi, H. Kumigashira, M. Oshima, H. Koinuma, *Appl. Phys. Lett.* **2004**, *85*, 272.

[39] Y. Bourlier, M. Frégnaux, B. Bérini, A. Fouchet, Y. Dumont, D. Aureau, *ChemNanoMat* **2019**, *5*, 674.

[40] G. Panaccione, I. Vobornik, J. Fujii, D. Krizmancic, E. Annese, L. Giovanelli, F. Maccherozzi, F. Salvador, A. De Luisa, D. Benedetti, A. Gruden, P. Bertoch, F. Polack, D. Cocco, G. Sostero, B. Diviacco, M. Hochstrasser, U. Maier, D. Pescia, C. H. Back, T. Greber, J. Osterwalder, M. Galaktionov, M. Sancrotti, G. Rossi, *Rev. Sci. Instrum.* **2009**, *80*, 043105.

[41] J. J. Yeh, I. Lindau, *At. Data Nucl. Data Tables* **1985**, *32*, 1.

[42] C. Castán-Guerrero, D. Krizmancic, V. Bonanni, R. Edla, A. Deluisa, F. Salvador, G. Rossi, G. Panaccione, P. Torelli, *Rev. Sci. Instrum.* **2018**, *89*, 054101.

[43] L. Fitting Kourkoutis, Y. Hotta, T. Susaki, H. Y. Hwang, D. A. Muller, *Phys. Rev. Lett.* **2006**, *97*, 256803.

[44] T. Yamaguchi, S. Shibuya, S. Suga, S. Shin, *J. Phys. C Solid State Phys.* **1982**, *15*, 2641.

[45] G. van der Laan, I. W. Kirkman, *J. Phys. Condens. Matter* **1992**, *4*, 4189.

[46] R. Zimmermann, R. Claessen, F. Reinert, P. Steiner, S. Hüfner, *J. Phys. Condens. Matter* **1998**, *10*, 5697.

[47] S. Kalavathi, S. Amirthapandian, S. Chandra, P. C. Sahu, H. K. Sahu, *J. Phys. Condens. Matter* **2014**, *26*, 015601.

[48] S. C. Chen, K. Y. Sung, W. Y. Tzeng, K. H. Wu, J. Y. Juang, T. M. Uen, C. W. Luo, J. Y. Lin, T. Kobayashi, H. C. Kuo, *J. Phys. D. Appl. Phys.* **2013**, *46*.

[49] H. Tan, J. Verbeeck, A. Abakumov, G. Van Tendeloo, *Ultramicroscopy* **2012**, *116*, 24.

[50] Q. Lu, S. R. Bishop, D. Lee, S. Lee, H. Bluhm, H. L. Tuller, H. N. Lee, B. Yildiz, *Adv. Funct. Mater.* **2018**, *28*, 1803024.

[51] A. Gloter, V. Serin, C. Turquat, C. Cesari, C. Leroux, G. Nihoul, *Eur. Phys. J. B* **2001**, *22*, 179.

[52] F. Tavani, M. Busato, L. Braglia, S. Mauri, P. Torelli, P. D'Angelo, *ACS Appl. Mater. Interfaces* **2022**, *14*, 38370.

[53] M. Wu, J.-C. Zheng, H.-Q. Wang, *Phys. Rev. B* **2018**, *97*, 245138.

[54] J. Macías, A. A. Yaremchenko, J. R. Frade, *J. Alloys Compd.* **2014**, *601*, 186.